NIH Public Access
Author Manuscript
*J Control Release*. Author manuscript; available in PMC 2012 November 7.

Published in final edited form as:
*J Control Release*. 2011 November 7; 155(3): 358–366. doi:10.1016/j.jconrel.2011.06.032.

# A Novel Nested Liposome Drug Delivery Vehicle Capable of Ultrasound Triggered Release of its Payload

**Stuart Ibsen**[1,*,+], **Michael Benchimol**[2,+], **Dmitri Simberg**[3], **Carolyn Schutt**[1], **Jason Steiner**[4], and **Sadik Esener**[5]

[1]Department of Bioengineering, Moores Cancer Center, University of California San Diego, 3855 Health Sciences Dr. # 0815, La Jolla, CA 92093-0815,

[2]Department of Electrical & Computer Engineering, Moores Cancer Center, University of California San Diego, La Jolla, CA 92093 USA

[3]Moores Cancer Center, University of California San Diego, La Jolla, CA 92093 USA

[4]Department of Material Science, Moores Cancer Center, University of California San Diego, La Jolla, CA 92093 USA

[5]Department of Nanoengineering, Moores Cancer Center, University of California at San Diego, La Jolla, CA 92093 USA

## Abstract

The use of focused ultrasound can be an effective method to locally highlight tumor tissue and specifically trigger the activation of echogenic drug delivery vehicles in an effort to reduce systemic chemotherapy side effects. Here we demonstrate a unique ultrasound triggered vehicle design and fabrication method where the payload and a perfluorocarbon gas microbubble are both encapsulated within the internal aqueous space of a liposome. This nested lipid shell geometry both stabilized the microbubble and ensured it was spatially close enough to interact with the liposome membrane at all times. The internal microbubble was shown to fragment the outer liposome membrane upon exposure to ultrasound at intensities of 1 - 1.5 MPa. The focused ultrasound allowed the release of the internal payload to localized regions within tissue phantoms. The vehicles showed high payload loading efficiency of 16%, stability in blood of several hours, and low level macrophage recognition in vitro. High speed fluorescent videos present the first optical images of such vehicles interacting with ultrasound. This ability to open the outer membrane in small regions of deep tissue could provide a second level of spatial and temporal control beyond biochemical targeting, making these particles promising for in vivo animal studies.

### Keywords

burst release; ultrasound triggered release; focused ultrasound; microbubbles; triggered drug delivery

## 1. INTRODUCTION

Indiscriminate exposure of all cells in the body to a systemically administered chemotherapy drug is the main cause of harmful toxic side effects[1]. Certain drug delivery vehicles such as Abraxane for delivery of paclitaxel and liposomal Doxil for doxorubicin[2, 3] reduce

[*]Corresponding Author Phone (858) 534-9848, Fax: (858) 534-9830, sibsen@ucsd.edu .
[+]These authors contributed equally to this work

NIH-PA Author Manuscript
NIH-PA Author Manuscript
NIH-PA Author Manuscript

NIH-PA Author Manuscript

NIH-PA Author Manuscript

NIH-PA Author Manuscript

exposure of non-targeted cells to the drug while accumulating a therapeutic dose within the tumor. Passive accumulation in the tumor tissue due to the enhanced permeation and retention of the vasculature[2] coupled with slow drug release limits the bioavailability to non-tumor organs[4]. However, this slow release also limits the maximum levels of drug in the tumor[5], and nonspecific accumulation in healthy tissue remains a major hurdle[2].

The use of tumor targeting ligands has the potential to improve the preferential accumulation of these delivery vehicles in tumor tissue [6, 7]. The delivery requires endocytosis of the targeted vehicle with subsequent endosomal escape[8, 9]. However, saturation of the targetable receptors limits the targeting efficiency. Also, tumor “receptors” are rarely unique to the tumor [10] and the targeted particles accumulate in other healthy tissues, especially in the liver and spleen, causing local toxicity [11].

To address the difficulties of pure biochemical targeting, an independent non-biochemical trigger is required to cause instantaneous drug release only from the particles that have accumulated in the tumor tissue. Ultrasound is an attractive trigger candidate due to its low cost, wide availability, its generation external to the body, and its independence from biochemical or physical properties of the tumor. It can be focused to small volumes of deep tissue on the order of several cubic millimeters[12] to avoid healthy tissue. It is non-ionizing, and does not damage tissue as long as the exposure is kept below 720 $mW/cm^2$ [13, 14].

The best particles to respond to ultrasound at safe exposure levels are gas-filled microbubbles[15] already approved for human use as ultrasound contrast agents [16, 17]. Ultrasound causes large size fluctuations in microbubbles due to the large density difference between the compressible gas and the surrounding water, which induces microstreaming of fluid around the microbubble and disrupts nearby membranes [18]. Microbubbles can also adiabatically implode (cavitate) producing a shockwave and water jets which can penetrate nearby membranes. This causes sonoporation and can facilitate delivery of DNA or drugs into cells[17, 19-21]. Significant work has been done to employ microbubbles as delivery vehicles in vivo [19, 21] without much success [22]. This is likely attributed to extremely short circulation times of microbubbles in vivo (3-15 min half-life [22]) and to limited payload capacity.

Surface loading of a hydrophilic payload, such as DNA, is limited by the surface area of the microbubble[23-26] and leaves it exposed to degradation and potential immune system recognition. Hydrophobic payloads are carried in limited volumes of thickened lipid, polymer, or oil surrounding the microbubble [25, 27] but when fragmented the hydrophobic drug will be contained in relatively large lipid particles reducing diffusion rates.

Drug loaded liposomes have been attached to the surface of microbubbles[28], however the points of attachment can concentrate shear stress during transport through the microvasculature and destabilize the entire particle. Separate drug-loaded liposomes and microbubbles can be targeted to the same tissue, but successful delivery of the drug depends on very close co-localization of both particles because the cavitation shockwave is only effective at disrupting membranes within a few tens of microns. It is unlikely that both particles would be present in sufficient proximity and concentration to deliver a therapeutic dose.

To protect the microbubble and address the challenges described above, the microbubble and the payload can be encapsulated together within a protective outer liposome membrane shell. Previous efforts to incorporate gas bubbles into liposomes have used freeze drying techniques[29] or chemical reactions that create $CO_2$ microbubbles[30], but have very low yields. They also lack sufficient control over gas and payload entrapment, stability, and

NIH-PA Author Manuscript

NIH-PA Author Manuscript

NIH-PA Author Manuscript

internal geometry, resulting in a large distribution of properties. Such distributions reduce the effectiveness of ultrasound to activate the entire population. Premade microbubbles stabilized with a lipid monolayer can be made independently using standard probe sonication techniques which increases bubble half-life in storage and *in vivo*. Microbubbles of desired size ranges can be collected and subsequently encapsulated in liposomes.

The most common methods of liposome encapsulation involve exposure to vacuum, sonication, heating, and/or extrusion, all of which destroy microbubbles. Ethanol injection is gentle enough to allow the microbubbles to survive the encapsulation process but produces liposomes too small to encapsulate a microbubble[31]. Detergent dialysis methods[32] can make liposomes large enough to encapsulate microbubbles and are gentle enough to not destroy them in the process.

Here we demonstrate a new manufacturing method to reproducibly encapsulate and protect premade microbubbles in a liposome as shown schematically in Fig. 1a. This method is similar to detergent dialysis but uses organic solvents to dissolve the lipids. A slow diffusive introduction of water allows the lipid membranes to seal and encapsulate the large microbubbles. We refer to these malleable nested structures as SHockwavE-Ruptured nanoPayload cArriers (SHERPAs).

## 2. MATERIALS AND METHODS

### 2.1 Materials

L-α-phosphatidylcholine (EPC) from chicken eggs, distearoyl phosphatidylcholine (DSPC), distearoyl phosphatidylethanolamine-methyl poly(ethylene glycol) MW5000 (mPEG-DSPE), and cholesterol were purchased from Avanti Polar Lipids, Inc. (Alabaster, AL). 1,2-propanediol, glycerol, ethanol, and perfluorohexane were purchased from Sigma-Aldrich. All water was purified using the Milli-Q Plus System (Millipore Corporation, Bedford, USA). DiO was purchased from Biotium, Inc. CA. The PBS was purchased from Hyclone Laboratories Inc. (Logan, UT).

### 2.2 SHERPA production

**2.2.1 Lipid Preparation—**The SHERPAs were manufactured in a two step procedure with the microbubbles being formed through a probe sonication process and subsequently encapsulated in the outer liposome. The desired payload of nanoparticles or water soluble drug can be introduced in Solution 1, Solution 2, or in the PBS used for the final encapsulation step.

**Solution 1: Outer Liposome Lipid Solution:** A 1.5 mL eppendorf tube was filled with 76 μL of EPC in chloroform (26 mM)(20 mg $mL^{-1}$) and 10 μl of cholesterol in chloroform (100 mM)(387 mg $mL^{-1}$). The chloroform was removed by evaporation while vortexing under an argon stream. 125 μL of ethanol was then added and the solution was vortexed at 3200 rpm for 30 sec. To visualize lipid membranes, 5 μL of 1 mM DiO (Biotium, Hayward, CA) in ethanol was added.

**Solution 2: Microbubble Solution:** A 1.5 mL eppendorf tube was filled with 25 μL of DSPC in chloroform (51 mM) (40 mg $mL^{-1}$) and 20 μL mPEG5000-DSPE in chloroform (8.6 mM) (50 mg $mL^{-1}$). The chloroform was removed by evaporation while vortexing under an argon stream. Then 450 μL of 1,2-propanediol was added. The solution was vortexed at 3200 rpm for 30 sec, and then placed in a heating block at 60 °C.

NIH-PA Author Manuscript

NIH-PA Author Manuscript

NIH-PA Author Manuscript

After 10 minutes, the solution was vortexed at 3200 rpm for 10 sec, and 150 μL glycerol was added. The solution was gently vortexed for 30 sec, and then placed back into the 60 °C heating block. The heating, vortexing cycle was repeated until the glycerol was fully mixed in and the solution was homogeneous. This solution was then transferred to a 4 ml glass vial with a narrow neck. The neck of the glass vial was covered with parafilm to create a barrier and prevent loss of PFH gas during the violent sonication process.

The headspace of the container was filled with perfluorohexane gas using the method shown in Fig. 2 at 25 °C. 0.5 ml of the PFH liquid was first drawn into a 5 ml syringe. The plunger was then pulled all the way to the back of the syringe leaving 4.5 ml of air space. The syringe was rotated to coat all the walls of the syringe with the PFH several times to encourage fast vaporization of the PFH into the air. The metal needle of the syringe was bent at 130° from vertical and the syringe held upright as shown in Fig. 2A. The needle of the syringe was then inserted through the parafilm barrier and 4 ml of PFH/air mixture inside the syringe was injected into the air space as seen in Fig 2B. Care was taken to not inject any liquid PFH into the vial. The air that was originally in the vial head space was forced out of the vial through the needle track hole made in the parafilm.

As shown in Fig. 2C the tip of the probe sonicator (Fisher Scientific Model 100 Sonic Membrane Disruptor) was then inserted through the parafilm and positioned 1 mm below the surface of the lipid solution. The sonication power used was 25 W for 20 seconds. The temperature of the solution began at 25 °C but increased to approximately 40 °C at the end of the soniction. This bubble solution was put immediately on ice to help preserve the microbubbles and facilitate the formation of lipid sheets.

**2.2.2 Microbubble Encapsulation and SHERPA Formation—**After allowing Solution 2 to cool to room temperature, Solution 1 was added drop wise to Solution 2 under vortex at 3200 rpm. This new solution was Solution 3.

1.5 mL Eppendorf tubes were each filled with 200 μL of Solution 3. 100 μL of PBS was gently added to the bottom of each tube to initiate the closing of the lipid sheets and formation of the SHERPA. After 10 min, the tubes were rotated gently at an angle until the bubbles mixed thoroughly throughout the solution.

**2.2.3 Microbubble Stability—**Fig. 2D shows that once the sonication process began the only gas that could have been incorporated into the forming microbubbles was the PFH/air mixture. Control experiments showed greater long term stability for microbubbles made with the PFH gas and air mixture over those made with just pure air.

Allowing the PFH liquid to evaporate into the airspace of the syringe allowed the PFH gas to naturally come to equilibrium with the liquid PFH and the atmospheric gasses at atmospheric pressure. This process ensured that the PFH gas was present in a concentration that provided stability to the microbubble at atmospheric pressure and gas composition. Microbubbles made with no PFH would simply dissolve away and collapse. If the PFH gas concentration was too high then the PFH would recondense into a liquid droplet collapsing the microbubble. If the PFH gas concentration was too low then there would be a driving force for nitrogen to leave the microbubble and shrink its size to the collapse radius [33, 34].

For the purpose of these observational experiments the SHERPA were not stabilized with a PFH gas concentration against arterial pressure like the microbubbles used for ultrasound contrast imaging. The microbubbles described here were stabilized for atmospheric pressure and gas composition because these were the conditions they were exposed to while being tested in the ultrasound microscope setup. The microbubbles needed to be stabilized only

NIH-PA Author Manuscript

NIH-PA Author Manuscript

NIH-PA Author Manuscript

against atmospheric pressure because the Laplace pressures on the microbubbles were greatly reduced due to the reduction of interfacial tension caused by the lipid coating [35]. For in vivo experiments the microbubble manufacturing process described here could be easily modified to have the same PFH mixture already developed to stabilize for in vivo pressure conditions [33].

**2.2.4 Purification—**The desired microbubble-containing liposomes were separated from the empty liposomes by gentle centrifugation. The positive buoyancy of the entrapped microbubbles caused the actual SHERPAs to rise to the top of the reaction solution allowing them to concentrate. A Beckman Coulter Allegra X-15R Centrifuge was used at 524 g. The purification was done in an inverted syringe inside a 50 ml tube oriented so the SHERPA would rise against the plunger. The subnatant, containing mostly empty liposomes, could be expressed and replaced with fresh solution to purify the SHERPAs as well as wash them from any unreacted materials or unencapsulated payloads.

### 2.3 Retention Time of Doxorubicin

A sample of doxorubicin-loaded SHERPAs (.37 mg/mL DOX) was prepared, by dissolving 0.4 mg of doxorubicin hydrochloride (Jinan Wedo Industrial Co., Ltd. Shandong Province, China) in the bubble solution. The sample was diluted 1:20 by volume in PBS to improve dialysis performance. One sample of SHERPAs without DOX was prepared to determine the background fluorescence, and one solution of just the equivalent solvents and DOX was used to determine the dialysis rate of DOX.

Each sample (250 μL) was dialyzed against 1 L PBS using Spectra/Por cellulose ester membrane tubing with a molecular weight cutoff of 1MDa. The 1 MDa pore size was chosen because it was much larger than the DOX molecule, allowing unrestricted diffusion across the membrane. The smallest liposomes manufactured were too large to pass through these membrane pores so all of the liposomes were retained. When measuring drug retention time it was crucial that the dialysis rate was much faster than the SHERPA leakage rate, so the DOX would not build up in the fluid surrounding the liposomes inside the dialysis tubing. For each measurement, the relative concentration of doxorubicin within the dialysis tubing was determined by measuring the fluorescence with the TECAN Infinite 200 plate reader (Männedorf, Switzerland). The excitation and emission wavelengths were 475 and 595 nm respectively. The DOX-loaded SHERPA were analyzed at times 0, 0.5 hrs, 2 hrs, 6 hrs, and 24 hrs. For each time point, a separate sample was dialyzed.

### 2.4 Encapsulation Efficiency of IgG

To load the SHERPAs, mouse IgG was dissolved into the microbubble solution (solution 2) before the addition of water caused outer membrane sealing. A sandwich ELISA was used to assay the amount of free IgG. The background signal was determined by an identical sample with no IgG. For a positive control, IgG was added to the outside of this sample. Alternate liposomes were prepared by hydrating a lipid film with a solution containing IgG.

The difference between the sample and the positive control was taken to be the amount encapsulated. The percent encapsulation was calculated by dividing the difference by the background-adjusted positive control.

### 2.5 SHERPA characterization

**2.5.1 Ultrasound microscope equipment—**A custom system was developed to characterize the interaction of these SHERPAs with ultrasound. A water tank was used to couple the ultrasound to the SHERPA samples. Ultrasound was generated with a submersible Panametrics 2.25 MHz transducer (V305-Su, 1” sphericalfocus) using a

NIH-PA Author Manuscript

NIH-PA Author Manuscript

NIH-PA Author Manuscript

Panametrics BCU -58 - 6W waterproof connector cable. A needle hydrophone from Onda Corporation (HNP-0400 Broadband Needle Hydrophone AH - 2020-100 with hydrophone pre amp, 50kHz - 100 MHz, 0 +20 db.) was used to measure the sound field, and a Photron FASTCAM 1024 PCI acquired the image sequences. The National Instruments PCI 5412 arbitrary waveform generator was used to create different waveforms and was controlled using a custom designed LabVIEW 8.2 program. A 300 W amplifier from Vox Technologies (model number VTC2057574) was used to create acoustic intensities at the focal region of up to 1.6 MPa.

The samples being analyzed were held in a custom fabricated microwell chamber comprised of a coverslip and a slab of Polydimethylsiloxane (PDMS) with a 15 μm-deep molded well. The microwell was placed halfway in the water, with the coverslip above the surface for fluorescent imaging with a Nikon 100X oil objective. The PDMS served as a coupling medium for the ultrasound between the water bath and the sample well.

### 2.5.3 Phagocyte uptake experiments

**2.5.3.1 Macrophage Culture:** J774A.1 mouse macrophages were purchased from American Type Culture Collection (ATCC) Manassas, VA, USA. Cells were cultured in a 75 $cm^2$ flask with DMEM containing 10% Fetal Bovine Serum, glutamate and penicillin-streptomycin antibiotics (all purchased from Gibco, Invitrogen, Carlsbad, CA). SHERPAs and fluorescent beads (FluoSpheres, Invitrogen, Carlsbad, CA) were incubated with the macrophages for 1 hr.

**2.5.3.2 Dendritic Cell Culture:** Peripheral Blood Mononuclear Cells (PBMCs) were isolated from the blood of normal volunteers (San Diego Blood Bank) over a Ficoll-Hypaque (Amersham Biosciences, Uppsala, Sweden) density gradient. To generate dendritic cells (DCs), PBMCs were allowed to adhere to culture plates for 1h. The non-adherent cells were washed off and the adherent cells were cultured in RPMI 1640 medium supplemented with 2 mM L-glutamine (GIBCO-BRL Life Technologies; Grand Island, NY, USA), 50 mM 2-mercaptoethanol (Sigma, St. Louis, MO, USA), 10 mM HEPES (GIBCO-BRL), penicillin (100 U/mL),streptomycin (100mg/mL) (GIBCO-BRL) and 5% human AB serum (Gemini Bio Products West Sacramento, CA, USA), supplemented with 1000 U GM-CSF/mL (Cardinal Health, Dublin, OH, USA) and 200U IL-4/mL (R&D Systems, Minneapolis, MN ) at days 0, 2, and 4. Immature DCs were harvested on days 5-7. These N178 human dendritic cells were incubated with SHERPAs for 1 hr, and FITC-dextran (IVGND1845, Invitrogen, Carlsbad, CA) was used as a positive control. Results were analyzed with FACS using the FACSCalibur system (BD Biosciences, San Jose, CA) and fluorescence microscopy.

## 3. RESULTS

### 3.1 SHERPA Structure

The dialysis-based manufacturing process described above produced the desired SHERPA structure consisting of a nested 5 μm liposome containing a 1 μm microbubble as shown schematically in Fig. 1a and with fluorescence microscopy in Fig. 1b. The Brownian motion of the microbubble and payload of the SHERPA was contained entirely within the outer membrane as shown in a series of sequential pictures in Fig. 1c. These structures were observed to be stable for several days.

### 3.2 SHERPA Production

**3.2.1 Microbubble Formation—**The probe sonication of the heated glycerol and 1,2-propanediol mixture containing dissolved DSPC and mPEG5000-DSPE successfully created microbubbles coated with a stabilizing lipid monolayer. This increased their resistance to the

NIH-PA Author Manuscript

NIH-PA Author Manuscript

NIH-PA Author Manuscript

subsequent introduction of ethanol. DSPC was chosen because its long saturated tails result in a high $T_c$ of 55 °C. The brush layer created by the mPEG5000-DSPE helped increase SHERPA stability by preventing microbubbles from merging with each other and the outer liposome membrane. Perfluorohexane was chosen as the gas due to its established biocompatibility and low water solubility which increased the microbubble stability[26]. The high viscosity environment of the glycerol and 1,2-propanediol increased the concentration of microbubbles (~$10^8$/mL) by reducing their direct physical contact until they reached a more stable state.

**3.2.2 Microbubble Encapsulation—**The addition of the ethanol solution containing the egg PC lipid, cholesterol, and the lipophilic dye DiO to the microbubble solution drop wise under high vortex created lipid structures that intermixed with the microbubbles as shown in Fig. 3a. These structures appear to be unclosed lipid sheets whose free ends were stable under these solvent conditions. The viscosity of the solvent was important because it slowed the diffusion of added water into the region of these lipid sheets, making their free ends slowly unstable over several minutes. The increasing instability of the free ends caused the sheets to seal with themselves and neighboring sheets encapsulating the intervening microbubbles to form SHERPAs as shown in Fig. 3b. Fig. 3c shows a magnified view with several SHERPAs present. Egg PC was chosen because its very low transition temperature ($T_c$) of −15 °C increased the flexibility and fluidity of the outer membrane, allowing the lipid sheets to seal. The flexibility could also help increase particle circulation time by allowing easier passage through the microvasculature. The cholesterol amount was optimized to increase stability of the outer liposome and improve drug retention time. Some of the mPEG5000-DSPE from the microbubble solution was also incorporated into the outer membrane. This was demonstrated by preventing charge interactions between SHERPAs doped with positively charged DOTAP lipid and cell surfaces. SHERPAs that were doped with DOTAP but did not have mPEG5000-DSPE attached readily to the surface of HUVEC cells. This indicates that the external surface of the SHERPAs were PEGylated and able to maintain a steric separation from the cells. This property is crucial to prolonging in vivo circulation time.

The large microbubbles shown in Fig. 3a disapeared in Fig. 3b and 3c because the added water made the solution less viscous. The larger bubbles floated quickly to the top, where they aggregated and destabilized. The 1-2 μm diameter microbubbles of choice rose more slowly and were much more stable when exposed to increasing concentrations of water in the formation process.

### 3.3 Encapsulation and Retention Time of Doxorubicin

One fundamental property of a drug delivery vehicle is its ability to contain its payload while in transit. The outer lipid membrane sheets of the SHERPA which close around the microbubble must seal to encapsulate a drug such as doxorubicin (DOX). DOX is currently dose limited by its cardiotoxic side effects, especially when administered systemically in free form[36-38]. DOX can be incorporated into the SHERPAs by its addition to the bubble solution, or to the water during the final formation step. The concentration of the DOX inside the SHERPA is the same as the concentration of the drug in these preparation solutions because this solution is encapsulated within the SHERPA along with the microbubbles. The SHERPA can be loaded with higher concentrations of DOX by using higher concentrations in the preparation solutions.

The encapsulation of DOX is shown in Fig. 4a. The retention time of free DOX was determined by dialyzing DOX-loaded SHERPAs against PBS, and measuring the DOX concentration over time from the fluid within the dialysis tubing. For passively loaded DOX,

NIH-PA Author Manuscript

NIH-PA Author Manuscript

NIH-PA Author Manuscript

the release followed an exponential decay with tight correlation. The retention half-life was 4.74 hours, and is in good agreement with the literature for other liposomes loaded with free DOX [39]. In the future, the retention time of DOX can be increased 10 times or more from this value by inducing the DOX to form crystals inside the liposomes by using proper pH gradients [39].

### 3.4 Encapsulation Efficiency of Microbubbles and Biomolecules

To evaluate the encapsulation efficiency of the SHERPA, mouse IgG was used as a model large biomolecule payload. An ELISA was performed to calculate the percent loading of IgG (150 kD, ~5 nm) into the SHERPAs. The samples were added directly to capture antibodies after formation, to minimize experimental error. Only free IgG was accessible to bind capture antibodies and contributed to the ELISA signal. The mean percentage of the entire volume of the preparation solution that was encapsulated within the SHERPA outer liposome was 16%. This was high for passive entrapment and much higher than the 2.5% measured for the liposomes prepared by thin film hydration [40] as shown in Fig. 4b. This is likely due to the larger size of the SHERPA liposomes and the fact that the lipids sheets are well suspended with the payload before sealing.

The encapsulation efficiency of the microbubbles into the SHERPA outer liposomes was lower (1-5%) because the IgG was small enough to fit into any sized SHERPA but the microbubbles were on the micron size and could only fit into the larger liposomes. However, these microbubble-containing SHERPAs were easily separated from the empty liposomes by buoyancy driven methods, since the microbubble inside reduces the overall density of the SHERPA compared to empty liposomes and bulk solution.

### 3.5 SHERPA Interaction with Ultrasound

**3.5.1 Ultrasound Intensity Level of 1.5 MPa—**The custom built high speed ultrasound microscope setup described in the methods section was used to observe the interaction of the fluorescently labeled SHERPA with ultrasound. Cavitation of the internal microbubble was observed at ultrasound intensity levels of 1.5 MPa as shown in Fig. 5a. Here the microbubble underwent a violent implosion producing a shockwave that fragmented the fluorescent lipid outer membrane into a cloud of fine debris. It is important to note that an empty liposome was present right next to the SHERPA as shown in Fig. 5a frame 1. This empty liposome contained no microbubble and was exposed to the same ultrasound pulse that cavitated the SHERPA, but had no visible reaction or disruption of the membrane. This shows that the ultrasound exposures required to cavitate the microbubbles would not harm the membranes of cells even in the focal zone. This localized effect of the cavitation on surrounding membranes illustrates the importance of the co-localization of the liposome and microbubble. A jet of debris material was also ejected from the site of cavitation as seen in frame 3 of the sequence. Fluid ejection is a well documented mode of microbubble cavitation[41].

**3.5.2 Ultrasound Intensity Levels Below 1 MPa—**A second mode of interaction between SHERPAs and ultrasound at levels below 1 MPa was observed in which the microbubble did not undergo cavitation, but instead had a less violent response. The size modulation of the bubble initiated an opening and unfolding of the SHERPA outer membrane as shown in Fig. 5b, probably due in part to microstreaming[41]. These free ends made the open membrane an unstable high energy structure.

**3.5.3. Localized SHERPA Activation—**The localized activation of SHERPA only near the focal region of the ultrasound was demonstrated in an agar tissue phantom using a biotin/avidin binding scheme. An agar gel was prepared with a 1 mm diameter channel molded

NIH-PA Author Manuscript

NIH-PA Author Manuscript

NIH-PA Author Manuscript

through the center to simulate a blood vessel which was coated with avidin. SHERPAs were made with DSPE-PEG2000-Biotin so the biotin was present on both the inner and outer surface of the SHERPA outer membrane. Biotins on the outside of the SHERPA were blocked by incubation with an excess of free avidin. The outer membrane was stained with DiO for visualization and the SHERPAs were introduced into the channel. The agar blocks were then insonified with focused ultrasound of various intensities. The control agar block showed very little nonspecific binding of the SHERPA to the walls of the channel after being washed with water as shown in Fig. 5c. Low intensity ultrasound ruptured the SHERPA only in the focal region, creating fluorescent membrane fragments with exposed free biotin that was originally on the inner leaflet of the SHERPA membrane. These fragments were then able to bind to the avidin coated walls of the channel allowing them to remain on the channel surface after it was flushed with water. Higher intensity ultrasound ruptured a larger number of SHERPA resulting in a higher fluorescent signal as well as creating a larger region of activation.

### 3.6 SHERPA Stability in Biological Fluids

SHERPA stability was evaluated by dilution into a blood sample followed by fluorescent microscopy. Intact SHERPAs were observed for up to two hours. Brownian motion caused the SHERPAs to interact with the surrounding red blood cells (RBCs), demonstrating their membrane flexibility. Much like the cells, they appeared to change their shape to pack closely with neighboring groups of RBCs a shown in Fig. 6a. The flexibility can potentially help reduce uptake from the spleen by mimicking the ability of RBCs to squeeze through the filtration system. No attachment or clotting induction of the SHERPAs on the RBCs was observed. Insonification with focused ultrasound ruptured SHERPA in the focal region allowing the biotin on the inside to bind to the surface of the channel. Higher intensity focused ultrasound created more activation and widened the range of SHERPA rupture causing larger deposition.

### 3.7 Macrophage Uptake of SHERPA

An effective drug carrier must be able avoid clearance by phagocytes for a sufficient period of time to reach its target. This nested design has a smooth PEG coated outer surface which presents less of a target for the immune system. J774 mouse macrophages were used to model the uptake of particles and liposomes fabricated by our method. SHERPA membranes were labeled green, and red Fluosphere beads were used as a positive control to show that the incubation solution did not inhibit the function of the macrophage. After 1 hr of incubation, macrophages were inspected by fluorescence microscopy. Fig. 6b shows strong macrophage uptake of red Fluospheres with no visible phagocytosis of SHERPAs.

SHERPAs were also incubated with N178 human dendritic cells and analyzed by FACS and fluorescence microscopy. The FITC-dextran control was contained within 96.9% of cells, whereas only 3.49% of cells contained fluorescently labeled SHERPAs. Scatter data showed no evidence of cell death. This indicates the possibility that the SHERPAs will have a low clearance rate from the immune system.

## 4. DISCUSSION

The SHERPA nested geometry has several attractive features as a drug delivery vehicle. The smooth continuous outer liposome with its PEG coating protects the internal microbubble and payload from degradation, reduces immune system recognition, and creates far greater loading capacity than microbubbles alone. The surface-to-volume ratio is far less than that of nanoliposomes which allows higher surface densities of targeting ligands to be used to increase targeting efficiency without the risk of receptor saturation. The materials used in

NIH-PA Author Manuscript

NIH-PA Author Manuscript

NIH-PA Author Manuscript

the construction of SHERPAs are bioresorbable and the perfluorocarbon gas can be cleared through exhalation.

The SHERPA are intended for intravenous injection which allows the SHERPA and the payload to penetrate every region of the tumor where the vasculature reaches, as opposed to an intratumoral injection where the SHERPA would be limited in their mobility from the injection site. The flexibility of the outer membrane can mimic the flexibility of red blood cell membranes and could help to increase circulation time of the SHERPA by allowing easier passage through the microvasculature. The SHERPA drug delivery vehicles themselves are not meant to extravasate from circulation into the tumor tissue. The main role of the SHERPA is to bring a highly concentrated payload into the tumor region through the vasculature. The payloads consisting of therapeutic nanoparticles or drug molecules are capable of extravasation once released from the SHERPA, especially inside the tumor region due to the “leaky” vasculature. The release of payload from the SHERPA located in the vasculature of the tumor will expose both the endothelial cells and the tumor tissue itself to the payload. Future work will explore the circulation time of these particles and the effect of focused ultrasound on payload delivery from the circulating particles to selected tissue regions.

The nested SHERPA structure always keeps the microbubble, large payload, and cell membrane in close proximity, increasing the chance for sonoporation[42] which is initiated by the cavitation event. Simultaneous pore formation in the cell membrane and release of high concentrations of payload in the same region could allow payload to travel down its concentration gradient into the cells, bypassing the need for endocytosis, and endosomal escape. With the resolution of focused ultrasound on the order of several cubic millimeters, SHERPAs residing in surrounding healthy tissue will be unaffected. They will break down gradually, diluting their payloads into the blood stream, making cellular delivery much less effective, and preventing accumulation of the drug[42]. This sonoporation effect may also occur during non-cavitation microbubble interactions from the microstreaming of fluid around the microbubble[41]. Transient holes formed in the cell surface can be on the order of 100 nm in diameter and allow for payload uptake to occur over several minutes[43].

## 5. CONCLUSIONS

Here we have demonstrated a process for consistent production of liposomes containing stabilized microbubbles. Though the overall structure is new, the outer liposome is amenable to standard functionalization and modifications well documented in the literature. These can increase their preferential accumulation in tumor sites to achieve maximum SHERPA concentration at the moment when the region is selectively insonified with ultrasound. This allows for both spatial and temporal control over activation with a burst release of a highly concentrated payload making these particles promising for in vivo studies.

## Acknowledgments

The authors are grateful for the insightful discussions with Ahmet Erten while conducting these experiments. The study was supported by the NCI Grant No. 5U54CA119335-05, and by the UCSD Cancer Center Specialized Support Grant P30 CA23100.

## REFERENCES

[1]. Shapiro C, Recht A. Side Effects of Adjuvant Treatment of Breast Cancer. N Engl J Med. 2001; 344(26):1997–2008. [PubMed: 11430330]

[2]. Gabizon AA. Pegylated Liposomal Doxorubicin: Metamorphosis of an Old Drug into a New Form of Chemotherapy. Cancer Investigation. 2001; 19(4):424–436. [PubMed: 11405181]

NIH-PA Author Manuscript

NIH-PA Author Manuscript

NIH-PA Author Manuscript

[3]. Miele E, Spinelli GP, Miele E, Tomao F, Tomao S. Albumin-bound formulation of paclitaxel (Abraxane® ABI-007) in the treatment of breast cancer. International Journal of Nanomedicine. 2009; 4:99–105. [PubMed: 19516888]

[4]. Gabizon A, Shmeeda H, Barenholz Y. Pharmacokinetics of pegylated liposomal Doxorubicin: review of animal and human studies. Clin Pharmacokinet. 2003; 42(5):419–436. [PubMed: 12739982]

[5]. Cheong I, Huang X, Bettegowda C, Diaz LA Jr. Kinzler KW, Zhou S, Vogelstein B. A bacterial protein enhances the release and efficacy of liposomal cancer drugs. Science. 2006; 314(5803): 1308–1311. [PubMed: 17124324]

[6]. Karmali PP, Kotamraju VR, Kastantin M, Black M, Missirlis D, Tirrell M, Ruoslahti E. Targeting of albumin-embedded paclitaxel nanoparticles to tumors. Nanomedicine. 2009; 5(1):73–82. [PubMed: 18829396]

[7]. Murphy EA, Majeti BK, Barnes LA, Makale M, Weis SM, Lutu-Fuga K, Wrasidlo W, Cheresh DA. Nanoparticle-mediated drug delivery to tumor vasculature suppresses metastasis. Proc Natl Acad Sci U S A. 2008; 105(27):9343–9348. [PubMed: 18607000]

[8]. Allen T. Ligand-Targeted Therapeutics in Anticancer Therapy. Nature Reviews Cancer. 2002; 2:750–763.

[9]. Ulrich AS. Biophysical Aspects of Using Liposomes as Delivery Vehicles. Bioscience Reports. 2002; 22(2):129–150. [PubMed: 12428898]

[10]. Park J, Hong K, Kirpotin D, Colbern G, Shalaby R, Baselga J, Shao Y, Nielsen U, Marks J, Moore D, Papahadjopoulos D, Benz C. Anti-HER2 Immunoliposomes: Enhanced Efficacy Attributable to Targeted Delivery. Clinical Cancer Research. 2002; 8:1172–1181. [PubMed: 11948130]

[11]. Moghimi SM, Hunter AC, Murray JC. Long-circulating and target-specific nanoparticles: theory to practice. Pharmacol Rev. 2001; 53(2):283–318. [PubMed: 11356986]

[12]. Zanelli CI, DeMarta S, Hennige CW, Kadri MM. Beamforming for Therapy with High Intensity Focused Ultrasound (HIFU) Using Quantitative Schlieren. IEEE Ultrasonics Symposium. 1993:1233–1238.

[13]. Wojcik G, Mould J, Lizzi F, Abboud N, Ostromogilsky M, Vaughan D. Nonlinear Modeling of Therapeutic Ultrasound. 1995 IEEE Ultrasonics Symposium Proceedings. 1995:1617–1622.

[14]. Barnett S, Ter Haar G, Ziskin M, Rott HD, Duck F, Maeda K. International Recommendations and Guidelines for the Safe Use of Diagnostic Ultrasound in Medicine. Ultrasound in Medicine and Biology. 2000; 26(3):355–366. [PubMed: 10773365]

[15]. Stride E, Saffari N. Microbubble ultrasound contrast agents: a review. Proc. Instn Mech. Engrs Part H: J. Engineering in Medicine. 2003; 217:429–447.

[16]. de Jong N, Bouakaz A, Frinking P. Basic acoustic properties of microbubbles. Echocardiography. 2002; 19(3):229–240. [PubMed: 12022933]

[17]. Von Bibra H, Voigt JU, Froman M, Bone D, Wranne B, Juhlin-Dannfeldt A. Interaction of Microbubbles with Ultrasound. Echocardiography. 1999; 16(7, Pt 2):733–741. [PubMed: 11175216]

[18]. Ferrara, R.P. Katherine; Borden, Mark. Ultrasound Microbubble Contrast Agents: Fundamentals and Application to Gene and Drug Delivery. Annu. Rev. Biomed. Eng. 2007; 9:415–447. [PubMed: 17651012]

[19]. Gao Z, Kennedy AM, Christensen DA, Rapoport NY. Drug-loaded nano/microbubbles for combining ultrasonography and targeted chemotherapy. Ultrasonics. 2007

[20]. Sun Y, Zhao S, Dayton PA, Ferrara KW. Observation of contrast agent response to chirp insonation with a simultaneous optical-acoustical system. IEEE Trans Ultrason Ferroelectr Freq Control. 2006; 53(6):1130–1137. [PubMed: 16846145]

[21]. Zhao YZ, Lu CT. Recent advances in the applications of ultrasonic microbubbles as gene delivery systems. Yao Xue Xue Bao. 2007; 42(2):127–131. [PubMed: 17518038]

[22]. Willmann JK, Cheng Z, Davis C, Lutz AM, Schipper ML, Nielsen CH, Gambhir SS. Targeted microbubbles for imaging tumor angiogenesis: assessment of whole-body biodistribution with dynamic micro-PET in mice. Radiology. 2008; 249(1):212–219. [PubMed: 18695212]

NIH-PA Author Manuscript

NIH-PA Author Manuscript

NIH-PA Author Manuscript

[23]. Kheirolomoom A, Dayton PA, Lum AF, Little E, Paoli EE, Zheng H, Ferrara KW. Acoustically-active microbubbles conjugated to liposomes: characterization of a proposed drug delivery vehicle. J Control Release. 2007; 118(3):275–284. [PubMed: 17300849]

[24]. Klibanov A. Microbubble Contrast Agents Targeted Ultrasound Imaging and Ultrasound Assisted Drug-Delivery Applications. Investigative Radiology. 2006; 41(3):354–362. [PubMed: 16481920]

[25]. Liu Y, Miyoshi H, Nakamura M. Encapsulated ultrasound microbubbles: Therapeutic application in drug/gene delivery. Journal of Controlled Release. 2006; 114:89–99. [PubMed: 16824637]

[26]. Lentacker I, De Geest B, Vandenbroucke R, Peeters L, Demeester J, De Smedt S, Sanders N. Ultrasound-Responsive Polymer-Coated Microbubbles That Bind and Protect DNA. Langmuir. 2006; 22:7273–7278. [PubMed: 16893226]

[27]. Unger E, McCreery T, Sweitzer R, Caldwell V, Wu Y. Acoustically Active Lipospheres Containing Paclitaxel: A New Therapeutic Ultrasound Contrast Agent. Investigative Radiolog. 1998; 33(12):886–892.

[28]. Kheirolomoom D, P. A, Lum A, Little E, Paoli E, Zheng H, Ferrara K. Acoustically-active microbubbles conjugated to liposomes: Characterization of a proposed drug delivery vehicle. Journal of Controlled Release. 2007; 118:275–284. [PubMed: 17300849]

[29]. Huang S, MacDonald R. Acoustically active liposomes for drug encapsulation and ultrasound-triggered release. Biochemica et Biophysica Acta. 2004; 1665:134–141.

[30]. Liu, R.; Wei, X.; Yao, Y.; Chai, Q.; Chen, Y.; Xu, Y. The preparation and characterization of gas bubble containing liposomes. Proceedings of the 2005 IEEE Engineering in Medicine and Biology 27th Annual Conference Shanghai; China. 2005.

[31]. Domazou A, Luisi P. Size Distribution of Spontaneously Formed Liposomes by the Alcohol Injection Method. Journal of Liposome Research. 2002; 12(3):205–220. [PubMed: 12604027]

[32]. Hosaka Y, Semba T, Fukai K. Artificial Assembly of Envelope Particles of HVJ (Sendai Virus). Fusion Activity of Envelope Particles. J Gen Virol. 1974; 25:391–404. [PubMed: 4374505]

[33]. Schutt E, Pelura T, Hopkins R. Osmotically-stabilized microbubble ultrasound contrast agents. Acad Radiol. 1996; 3:S188–S190. [PubMed: 8796558]

[34]. Schutt E, Klein D, Mattrey R, Riess J. Injectable Microbubbles as Contrast Agents for Diagnostic Ultrasound Imaging: The Key Role of Perfluorochemicals. Angew. Chem. Int. Ed. 2003; 42:3218–3235.

[35]. Borden MA, Pu G, Runner GJ, Longo ML. Surface phase behavior and microstructure of lipid/PEG-emulsifier monolayer-coated microbubbles. Colloids and Surfaces B: Biointerfaces. 2004; 35:209–223.

[36]. Singal PK, Iliskovic N. Doxorubicin-Induced Cardiomyopathy. The New England Journal of Medicine. 1998; 339(13):900–905. [PubMed: 9744975]

[37]. M. P, Olson RD. Doxorubicin cardiotoxicity: analysis of prevailing hypotheses. FASEB J. 1990; 4(13):3076–3086. [PubMed: 2210154]

[38]. Minotti G, Menna P, Salvatorelli E, Cairo G, Gianni L. Anthracyclines: Molecular Advances and Pharmacologic Developments in Antitumor Activity and Cardiotoxicity. Pharmacol Rev. 2004; 56:185–229. [PubMed: 15169927]

[39]. Mayer LD, Bally MB, Cullis PR. Strategies for Optimizing Liposomal Doxorubicin. Journal of Liposome Research. 1990; 1(4):463–480.

[40]. Berger N, Sachse A, Bender J, Schubert R, Brandl M. Filter extrusion of liposomes using different devices: comparison of liposome size, encapsulation efficiency, and process characteristics. International Journal of Pharmaceutics. 2001; 223:55–68. [PubMed: 11451632]

[41]. Young, F. Cavitation Imperial College Press; London: 1999.

[42]. Ohl C-D, Arora M, Ikink R, de Jong N, Versluis M, Delius M, Lohse D. Sonoporation from Jetting Cavitation Bubbles. Biophysical Journal. 2006; 91:4285–4295. [PubMed: 16950843]

[43]. Zarnitsyn V, Rostad C, Prausnitz M. Modeling Transmembrane Transport through Cell Membrane Wounds Created by Acoustic Cavitation. Biophysical Journal. 2008; 95(9):4124–4138. [PubMed: 18676653]

NIH-PA Author Manuscript

NIH-PA Author Manuscript

NIH-PA Author Manuscript

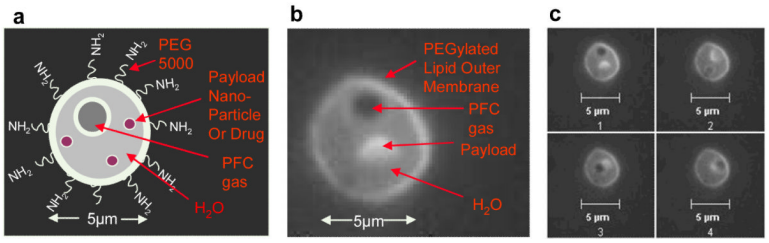


**Figure 1. SHERPA nested structural design**

(a) A schematic of the nested liposome SHERPA design. (b) Fluorescent image of a SHERPA resulting from the described manufacturing process. The payload is a small fluorescently labeled lipid membrane. (c) A series of sequential pictures taken of the SHERPA showing the microbubble and fluorescent lipid payload moving around inside due to Brownian motion. This confirms that the microbubble and payload were internal to the outer membrane and not just attached to the outside.

NIH-PA Author Manuscript
NIH-PA Author Manuscript
NIH-PA Author Manuscript



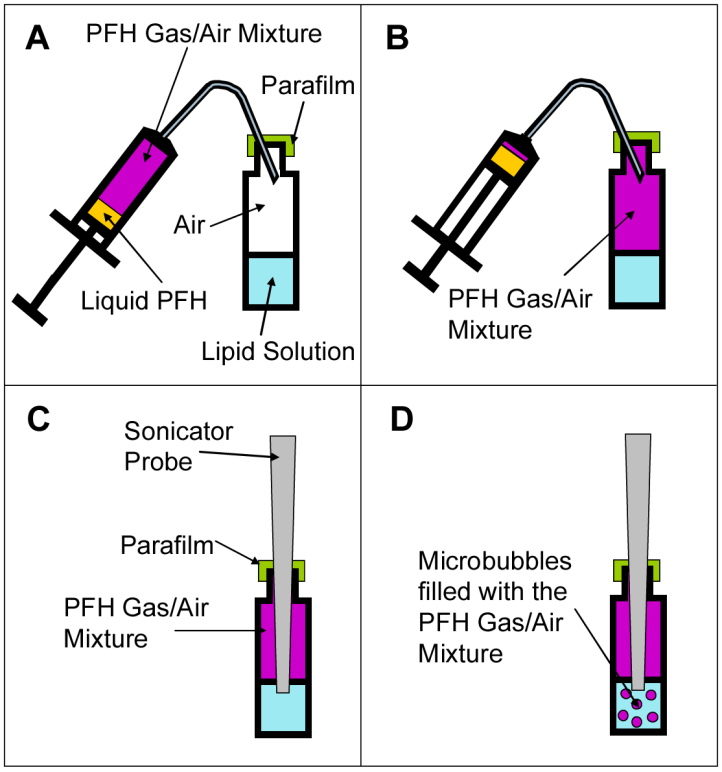


**Figure 2. Schematic representation of the manufacturing process for the PFH/air mixture filled microbubbles**

(a) A 5 ml syringe is filled with 0.5 ml of liquid PFH. The PFH is allowed to evaporate and mix with the air in the syringe until it reaches equilibrium. The top of the glass vial containing the lipid solution is covered with parafilm to reduce gas exchange from within the vial to the atmosphere (b) The PFH/air mixture is injected into the head space of the vial containing the lipid solution. Care is taken to prevent injection of any liquid PFH. The original air that was in the vial is displaced through the needle track hole made in the parafilm (c) The probe sonicator tip is inserted through the parafilm into the vial and the tip is positioned 1 mm below the surface of the lipid solution. (d) The probe sonicator is turned on and creates microbubbles which incorporate the PFH/air gas mixture in the headspace. These microbubbles are coated with the lipids from the solution.

NIH-PA Author Manuscript

NIH-PA Author Manuscript

NIH-PA Author Manuscript

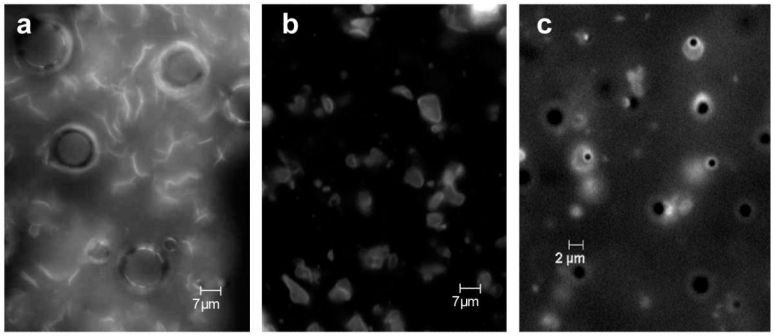


**Figure 3. SHERPA formation**

(a) The fluorescently labeled lipid structures mixed with the microbubbles shown before the final water addition step during SHERPA formation. The lipid structures appear to be open sheets whose free ends are stable under these mixed solvent conditions of glycerol, 1,2-propanediol, and ethanol. (b) After addition of water to the microbubble and ethanol mixture shown in Fig. 3a, the open free ends of the lipid sheets become energetically unstable and they seal with themselves and with the free ends of surrounding sheets encapsulating the intervening microbubbles. This magnification level is the same as in Fig. 3a. (c) This shows a close up of the SHERPAs just after formation.

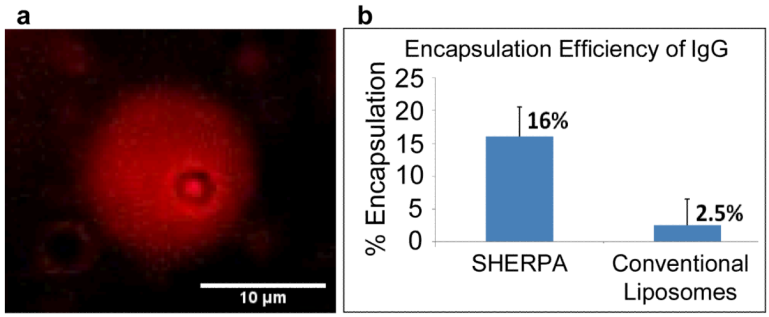


**Figure 4. SHERPA payload loading**

(a) Demonstration of doxorubicin loading. Red fluorescence from entrapped doxorubicin can be seen as a diffuse sphere. This liposome also contains a microbubble shown by the dark inner circle. (b) Efficient loading of a macromolecule, IgG, was demonstrated and quantified using ELISA. Other liposomes were prepared by standard methods for comparison.



NIH-PA Author Manuscript
NIH-PA Author Manuscript
NIH-PA Author Manuscript

NIH-PA Author Manuscript
NIH-PA Author Manuscript
NIH-PA Author Manuscript



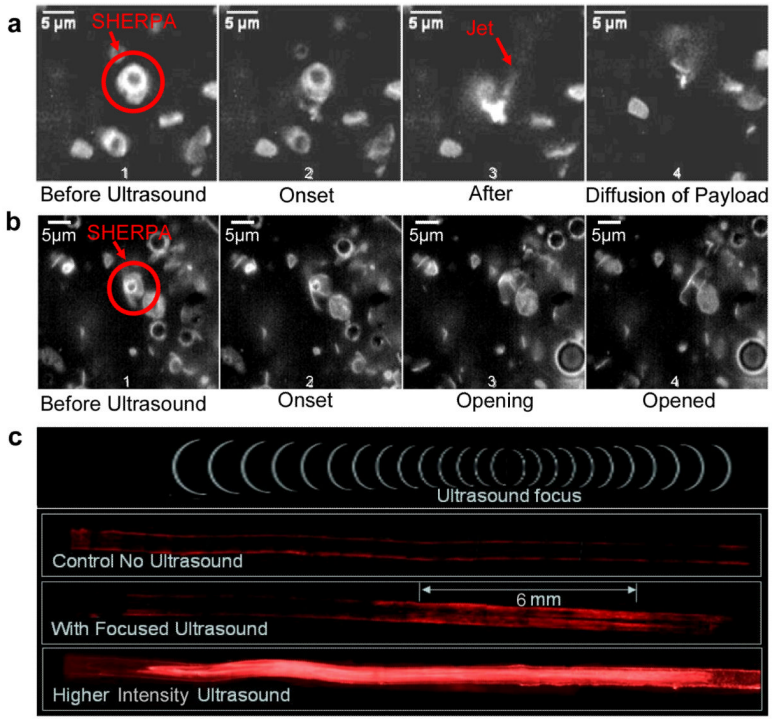


**Figure 5. Interaction of SHERPA with Ultrasound**

(a) Sequence of images showing a cavitation mode of ultrasound interaction with a SHERPA. Frame 1 shows the SHERPA before ultrasound exposure. Frame 2 shows the very onset of ultrasound exposure. Frame 3 shows the results just after the microbubble cavitation event creating a cloud of fluorescent debris. A jet of material has shot out from the main debris cloud. Frame 4 shows the diffusion of the membrane fragments 1.2 seconds after the cavitation event. (b) Sequence of images showing a popping type mode of SHERPA interaction with ultrasound. Frame 1 shows the SHERPA with its fluorescent outer membrane before exposure to ultrasound. Frame 2 shows the very onset of ultrasound exposure. Frame 3 shows the SHERPA membrane popping open on the lower right hand side and beginning to open up. Frame 4 shows the SHERPA fully opened up. (c) Images of ultrasound activation of SHERPA in simulated blood vessel channel within an agar block. The channel was coated with avidin and the SHERPA were functionalized with biotin. The biotin on the outside of the SHERPA was blocked with free avidin The control showed very little nonspecific binding of the fluorescently labeled SHERPA to the surface of the channel.

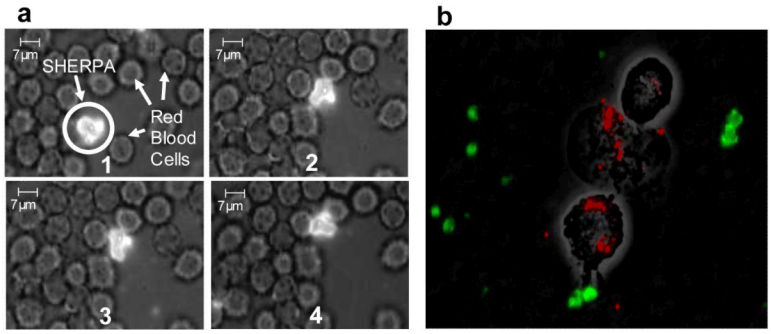


**Figure 6. SHERPA in vitro behavior**

(a) SHERPA interaction with red blood cells. The outer membrane of the SHERPA is very flexible and allows it to change shape so as to achieve close packing with surrounding red blood cells as shown through this sequence of pictures. The only driving force for this is Brownian motion. (b) Three J774 macrophages have engulfed nearly all the fluospheres (red). No liposomes (green) can be seen inside the macrophages.



NIH-PA Author Manuscript
NIH-PA Author Manuscript
NIH-PA Author Manuscript